Methane activation by chromium oxide cations in the gas phase: A theoretical study

ARTICLE *in* JOURNAL OF COMPUTATIONAL CHEMISTRY · JANUARY 2006

Impact Factor: 3.59 · DOI: 10.1002/jcc.20335 · Source: PubMed

3 AUTHORS:

Ivan Rivalta
Yale University
57 PUBLICATIONS **593** CITATIONS
SEE PROFILE

Nino Russo
Università della Calabria
512 PUBLICATIONS **7,920** CITATIONS
SEE PROFILE

Emilia Sicilia
Università della Calabria
151 PUBLICATIONS **1,937** CITATIONS
SEE PROFILE

Methane Activation by Chromium Oxide Cations in the Gas Phase: A Theoretical Study

IVAN RIVALTA, NINO RUSSO, EMILIA SICILIA

Dipartimento di Chimica and Centro di Calcolo ad Alte Prestazioni per Elaborazioni Parallele e Distribuite-Centro d'Eccellenza MURST, Università della Calabria, I-87030 Arcavacata di Rende, Italy

Received 29 April 2005; Accepted 1 July 2005
DOI 10.1002/jcc.20335
Published online in Wiley InterScience (www.interscience.wiley.com).

Abstract: Density Functional Theory, in its B3LYP formulation, was used to explore quantitative details of the potential energy hypersurfaces for the C—H bond activation reaction of methane by chromium dioxide cation. Both doublet ground and quartet excited states of the cation were considered, and all the minima and transition states localized along the paths leading to the formation of the experimentally observed products were characterized. All the calculated paths involve spin inversions that decrease the barrier heights of the involved transition states but do not play a significant role. Reaction pathways were also studied employing the nonhybrid BP86 functional, the reparametrized B3LYP* functional, and the CCSD(T) approach. Because other examples in the literature indicate that sequential ligation enhances the reactivity of bare transition metals cations, the state-selective reactivity of the chromium monoxide cation with respect to methane was also investigated and compared with that of the bare cation.

 J Comput Chem 27: 174–187, 2006

Key words: methane activation; chromium oxide cations

Introduction

Catalysts are used in most industrial processes to increase the rate of numerous reactions that even sometimes would not occur at the human time scale. They allow the use of milder chemical reaction conditions and lead to a huge saving in the fabrication costs. Renewed research to find more effective catalysts is then fundamental to improve efficiency and cut the costs. However, the detailed molecular mechanisms of many important catalytic processes in the condensed phase remain very often obscure. An approach that proved to be very fruitful in recent years is the study of reactivity in the gas phase. Indeed, because reactions are investigated under controlled conditions and without disturbing factors, precious insights into the elementary steps of more complex processes can be given.

C—H bond activation of methane and alkanes is the subject of considerable interest in recent transition metal catalytic chemistry.[1–9] Gas-phase experimental and theoretical investigations were by wide and large exploited as sources of complementary information. C—H and C—C bond activation of small hydrocarbons have been extensively studied in the laboratories of Armentrout[10] and Schwarz.[11] Many theoretical works on methane and C—H activation have been reported by Hoffmann,[12] Morokuma,[13] Goddard,[14] Siegbahn,[15] Ziegler,[16] Sakaki,[17] Hall,[18] and Cundari[19] groups. Early studies were mainly focused on the reactivity of bare metal ions, whereas an increasing number of reports appeared concerning the chemistry of metal ions bearing one or several ligands.[20–39]

Aside from the basic interest in ligand effects, oxo ligand specifically is object of study partly due to results coming from condensed phase studies of metal oxides. In particular, hydrocarbon oxidation is a field of great scope and economic volume. From an economic viewpoint, methane is a uniquely attractive target for controlled oxidation; its high abundance and low cost make it an ideal feedstock. For example, direct conversion to methanol would permit natural gas to be transported in a convenient and inexpensive liquid form.

The behavior of metal oxides is strongly influenced by the presence of multiple low-lying electronic states in these species. Therefore, during the course of chemical reaction that involves these species, the system can access these energetically quasi-

Correspondence to: E. Sicilia; e-mail: siciliae@unical.it

Contract/grant sponsor: Università degli Studi della Calabria

Contract/grant sponsor: MIUR

This article contains Supplementary Material available at http://www.interscience.wiley.com/jpages/0192-8651/suppmat

degenerate states and adapt to different bonding situations. Then, spin crossing between surfaces of different multiplicities can occur during the reaction and products formation arises from an interplay between spin inversion, barrier height, and thermodynamic factors on both surfaces. These reactions are defined in terms of the two-state reactivity (TSR) paradigm,[40] whose central idea was introduced, at first, by Armentrout and coworkers.[41,42]

In this work we have performed a detailed theoretical investigation of the possible mechanisms of the methane C—H bond activation by the cationic chromium dioxide (CrO_2^+). Density Functional Theory (DFT) was applied to characterize all the minima and first-order saddle points and to present a complete mechanistic scheme for this complex reaction sequence.

Because the comparison between the behaviors of chromium mono- and bis-ligated complexes seems to confirm that reactivity of the bare metal cations is enhanced by sequential ligation,[43,44] it results, in this context, to be interesting to check how the reactivity changes in going from the bare cation to the dioxide passing through the monoxide. Therefore, the potential energy surfaces (PESs) for the activation of the C—H bond of methane by the monoxide cation (CrO^+) have been also analyzed to this aim, whereas our previous work on this subject already covers the theoretical study of the methane activation by Cr^+ cation.[45]

A detailed examination of the reactions of bare CrO^+ with alkanes and alkenes, including methane, was carried out by Kang and Beauchamp,[24] which highlighted the peculiar behavior of this selective monoxide cation that appeared to not react with methane at thermal conditions, with respect to the other first-row transition metal monoxide cations. Schröder, Schwarz, and coworkers have systematically investigated the gas-phase reactivity of first-row transition metal monoxide cations with methane.[33] Not surprisingly, according to their oxophilicities, the early metal oxides do not react at all or hardly react, whereas late metal complexes are able to activate methane. Bridging these extremes are the MnO^+ and CrO^+ species. In particular, concerning the CrO^+ complex it is specified that it is able to oxidize alkanes larger than methane.

Reactivity of the high-valent Cr(V) dioxide cation CrO_2^+ with hydrocarbons was studied by Fiedler et al.[36] by means of ion-cyclotron resonance and sector-field mass spectrometry. In particular, considering the oxidation of methane, it results that CrO_2^+ is quite reactive, and product distribution of the reaction is given together with some hypotheses on the more conceivable reaction mechanisms to explain it. An extensive theoretical investigation of the methane–methanol conversion by first-row transition metal oxides, including CrO^+, was carried out by Yoshizawa et al.[46–48] at B3LYP level, whereas to our knowledge no theoretical study exists in literature concerning the reaction mechanism for the activation of methane by CrO_2^+.

Concerning the reactivity of cationic transition metal oxides, MO^+, interacting with methane three main reactions are observed to occur, with efficiencies and branching ratios varying across the periodic table. The mechanism proposed in this case to explain the observed experimental findings, involves formation of a key insertion intermediate $HO–M^+–CH_3$, which can dissociate to produce $MOH^+ + CH_3$. Alternatively, this intermediate can undergo migration of a methyl group or of another hydrogen atom to produce other two complexes, $H_2O–M^+–CH_2$ and $M^+–CH_3OH$, that subsequently dissociate to give the final products: $M^+ + CH_3OH$ or $MCH_2^+ + H_2O$.

On the other hand, mechanistic aspects, which can account for the experimental findings of the interaction of chromium dioxide with methane have been elucidated in this article, lacking any previous theoretical investigation of this subject. Because the cited reaction involves spin inversion in going toward products formation PESs corresponding to different spin multiplicities have been explored.

Computational Details

Geometry optimizations as well as frequency calculations for all the reactants, intermediates, products, and transition states were performed at the Density Functional level of theory, employing the Becke's three-parameter hybrid functional[49] combined with the Lee, Yang, and Parr (LYP)[50] correlation functional, denoted as B3LYP. Previous investigations indicated that the performance of the B3LYP DF in predicting numerous properties of transition metal containing systems is very satisfactory and, although the accuracy of the results is comparable to that obtainable by highly correlated *ab initio* methods, substantially less demanding computational efforts are required.[11i,51–58]

Orbital basis sets of DZVP[59] quality for chromium and TZVP[60] for the other atoms were used. The results of several theoretical works performed in the last years by Donostia[61] and Calabria[45,62] groups show that the B3LYP approach in conjunction with the above-mentioned basis sets is a reasonable choice for the theoretical exploration of the systems of interest to this work. However, difficulties have been known to occur with calculations involving both low- and high-spin configurations of open-shell transition metals[63–66] as is the case here. Therefore, additional calculations have been carried out using the very common Becke88 exchange functional[67] combined with Perdew86 correlation functional,[68] known as BP86, and the modified form of the B3LYP functional, in which the proportion of exact exchange admixture has been changed from 20 to 15%, named B3LYP*.[63] Energy changes were also evaluated performing single-point calculations at the B3LYP/DZVP optimized geometries and using a better basis set, TZVP+G(3df,2p), for the metal. Details concerning the employed triple-zeta quality basis set can be found elsewhere.[61]

No symmetry restrictions were imposed, whereas for each optimized stationary point vibrational analysis was performed to determine its character (minimum or saddle point). For transition states it was carefully checked that the vibrational mode associated to the imaginary frequency corresponds to the correct movement of involved atoms. Then, the zero-point vibrational energy (ZPVE) corrections, which are included in all relative energies, thermal energy corrections and entropy contributions were calculated at the B3LYP/DZVP level. The standard temperature (298.15 K) and pressure (1 atm) were used to obtain Gibbs free energies at the B3LYP/DZVP level.

The counterpoise corrections[69] have been calculated for all the ion–dipole complexes formed at the entrance channel of the considered reactions to correct binding energies (BE) for basis set superposition error (BSSE). The introduced corrections, less than 1.8 kcal/mol, do not change significantly the reported values.

For all the studied species we have checked $\langle S^2 \rangle$ values to evaluate whether spin contamination can influence the quality of the results. In all cases we have found that the calculated values differ from $S(S + 1)$ by less than 10%.

All the calculations reported in the present work have been carried out with the GAUSSIAN98/DFT code.[70] The program package was modified to easily change the amount of exact exchange admixture.

Finally, with the aim of comparison, single-point CCSD(T) calculations at B3LYP optimized equilibrium geometries were carried out to calculate the gaps between high and low spin states of Cr^+, CrO^+, and CrO_2^+ and the energy of the conversion reaction of methane to methanol by CrO^+. The triple-zeta quality basis set, TZVP+G(3df,2p), for the metal was used, and all the electrons were included into calculations. Single-point CCSD(T) calculations were also performed on the B3LYP geometries of all the minima and transition states localized along the pathways for the activation reactions of methane by chromium dioxide by using the same triple-zeta quality basis set and excluding from the correlation calculations the 1s electrons for O and the 1s, 2s, and 2p electrons for Cr. The applicability of the CCSD(T) approach to these systems was checked through the T1 diagnostic, which has been advanced as an indicator of multireference character in CCSD calculations.[71,72] T1 diagnostics exceeding the 0.02 value have to be considered suspicious. For simplicity, the B3LYP/TZVP+G(3df,2p)//B3LYP/DZVP and CCSD(T)/TZVP+G(3df,2p)//B3LYP/DZVP computations will be referred as B3LYP//B3LYP and CCSD(T)//B3LYP, respectively.

Table 1. Relative Energies (ΔE) at Different Levels of Theory of ^4D, $^2\Delta$, and $^4A''$ Excited States of Cr^+, CrO^+, and CrO_2^+ Species with Respect to the Corresponding ^6S, $^4\Pi$ and $^2A_1$ Ground States.

System	Method	ΔE	ΔE_1
Cr^+	B3LYP/DZVP	43.6	
	B3LYP*/DZVP	39.4	
	B3LYP/TZVP+G(3df,2p)	38.8	
	BP86/DZVP	38.0	
	CCSD(T)/TZVP+G(3df,2p)	47.3	
	Exp[a]	56.7	
CrO^+	B3LYP/DZVP	23.6	30.5
	B3LYP*/DZVP	20.2	34.3
	B3LYP//B3LYP	19.7	34.6
	BP86/DZVP	11.0	46.3
	CCSD(T)//B3LYP	17.8	33.2
CrO_2^+	B3LYP/DZVP	21.2	
	B3LYP*/DZVP	25.1	
	B3LYP//B3LYP	19.6	
	BP86/DZVP	36.4	
	CCSD(T)//B3LYP	27.3	

The relative energy (ΔE_1) of $^6\Pi$ excited state of CrO^+ with respect to the $^4\Pi$ ground state is also reported. All the values are in kcal/mol.
[a]Ref. 73.

Results and Discussion

Excitation Energies

For the reactions of interest three gaps between high and low spin states merit a discussion, that is the relative energies of the excited $^4A''$, $^2\Delta$ and $^6\Pi$ and ^4D states of CrO_2^+, CrO^+, and Cr^+, respectively, with respect to the corresponding $^2A_1$, $^4\Pi$, and ^6S ground states. In Table 1 are collected the computed excitation energies at all the employed levels of theory. T1 diagnostics greater than 0.02 were obtained for CrO_2^+ species. The unique experimental value existing in literature is the excitation energy of the sextet of Cr^+ toward the quartet state. The ground state of Cr^+ is of ^6S symmetry and arises from the configuration $3d^5$, while the first excited state is of ^4D symmetry, arising from the configuration $4s3d^4$, and lies 43.6 kcal/mol above. The best fitting with respect to the experimental value[73] is obtained at CCSD(T) level of theory. A comparison between the three used density functionals shows a general agreement even if the most satisfactory prediction is obtained at B3LYP/DZVP level.

A low-spin quartet ground state was assigned from a long time to CrO^+,[74–76] even if controversial remained the definitive assignment of a $^4\Pi$ or a $^4\Sigma$ electronic state. Our B3LYP/DZVP calculations give the $^4\Pi$ state as the ground one with $^2\Delta$ and $^6\Pi$ excited states lying 23.6 and 30.5 kcal/mol above, respectively. All the used approaches, including CCSD(T), agree between themselves, being the most different values those calculated with the pure BP86 functional. This result is reminiscent of observation[63] that pure functionals destabilize high spin states with respect to hybrid ones that show a preference for high-spin states.

Finally, the B3LYP/DZVP level calculates chromium dioxide cation to have a $^2A_1$ ground state corresponding to a bent C_{2v}-symmetrical structure with two Cr—O double bonds. The first excited state is the $^4A''$, which lies 21.2 kcal/mol above and corresponds to a bent structure with one double and one single Cr—O bonds. The computed B3LYP/DZVP energetical gap is lower than that of 33.2 kcal/mol previously obtained by Fiedler et al.[36] using the CASPT2D method. A better agreement with the CASPT2D value is found using all the other approaches except at B3LYP//B3LYP level. The next quartet closest state is the $^4B_2$ one that lies 39.9 kcal/mol above the doublet ground state at the same B3LYP/DZVP level of theory. More details on geometrical parameters of ground and excited states of dioxide are shown in Figure 1.

Activation of the C—H Bond of Methane by CrO^+

The more probable mechanism of the reaction of the first-row metal oxide cations with methane, consistently with experimental observations, involves as key features: formation of the insertion intermediate, $HO–M^+–CH_3$, and crossing between surfaces of different multiplicity. In Figure 2 are reported the computed B3LYP/DZVP PESs for the C—H bond activation by CrO^+ in both quartet and sextet states. Besides the PESs for conversion of methane to methanol also those for the minor channel leading to CrO^+ and H_2O products are shown. In addition, with the aim of comparison with analogous paths for the bare and dioxide cations, the energy diagrams for hydrogen elimination is presented in the same Figure 2. All the geometrical parameters of minima and

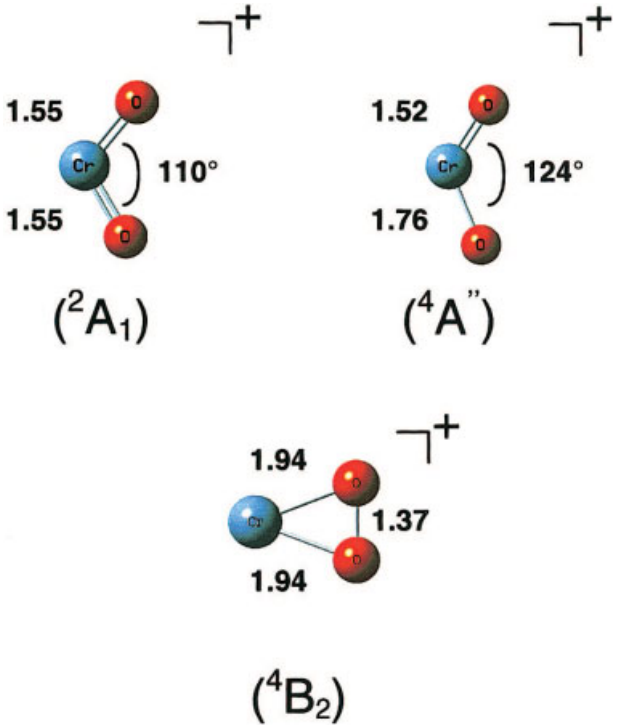

Figure 1. B3LYP/DZVP geometrical parameters of chromium dioxide cation in its ground $^2A_1$ and excited $^4A''$ and $^4B_2$ states. Bond lengths are in angstrom and angles in degrees. [Color figure can be viewed in the online issue, which is available at www.interscience.wiley.com.]

transition states are given in Figures S1–S2 (Supporting information).

The conversion reaction of methane to methanol begins with reactants in a low-spin quartet state. The next steps, that is, formation of the first ion–molecule complex, CrO^+–CH_4, and of the insertion intermediate, HO–Cr^+–CH_3, through the four-center transition state TS1, take place along the same quartet surface. Indeed, due to the presence of two covalent O—Cr and Cr—C bonds, two of the valence electrons of the metal are involved in bonding leading to a low-spin ground state for the HO–Cr^+–CH_3 intermediate. The transition state, TS1, is calculated to lie barely below the entrance channel dissociation limit. A barrier of −0.3 kcal/mol indicates that at thermal conditions the energy content initially present is hardly enough to overcome the barrier and generate the complex H–CrO^+–CH_3. Close to the transition state TSOH, which by means of the insertion of the OH group into the metal–carbon bond leads to the Cr^+–OH–CH_3 product complex, the relative order of the sextet and quartet states is reversed and a surface crossover occurs. The complex Cr^+–OH–CH_3 in the sextet ground state lies 56.2 kcal/mol lower in energy with respect the reactants dissociation limit and the barrier to exceed to obtain it is calculated to lie 13.6 kcal/mol below the same reference point. Final products barrierless formation takes place directly from intermediate Cr^+–OH–CH_3 and is exothermic by 17.5 kcal/mol. The exothermicity of the conversion of methane to methanol by CrO^+ calculated by us is overestimated with respect the values

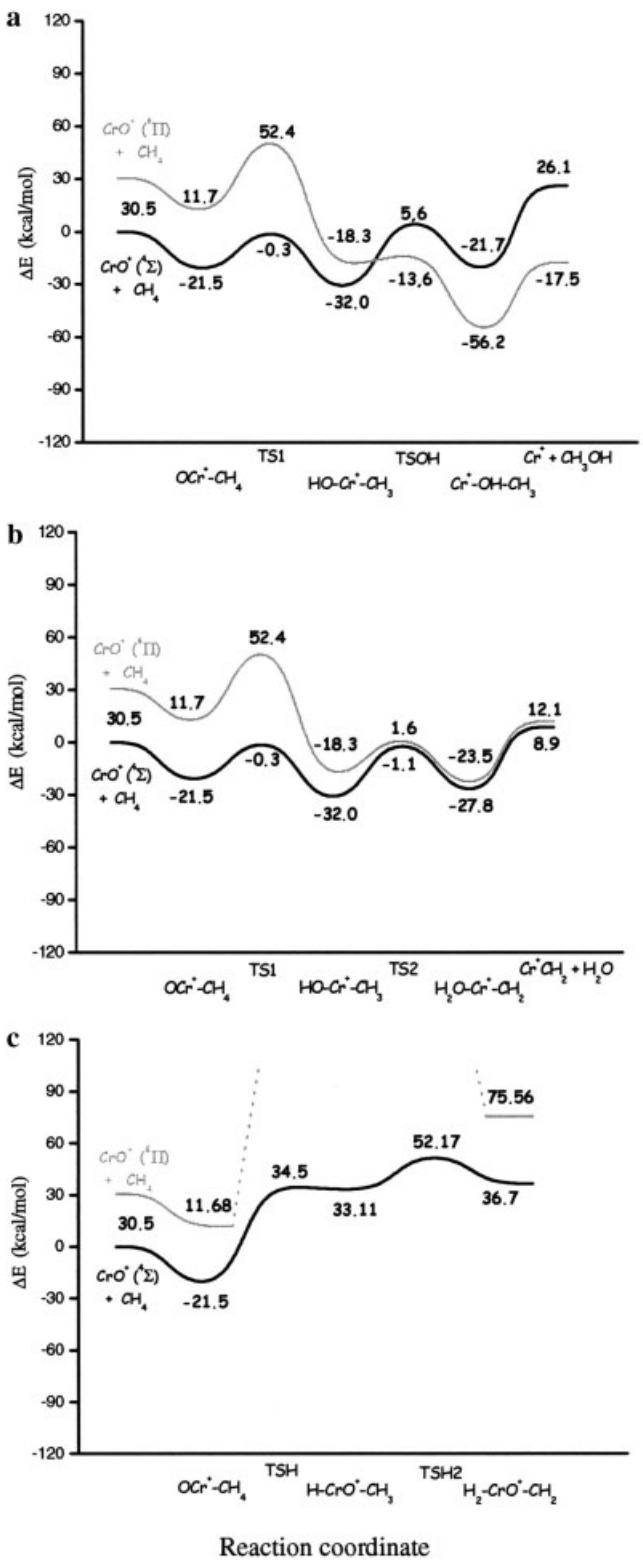

Figure 2. B3LYP/DZVP potential energy surfaces for the reaction of quartet and sextet states of CrO^+ with CH_4 for (a) conversion to methanol, (b) dehydration, and (c) dehydrogenation. Energies are in kcal/mol and relative to the ground-state reactants.

Table 2. Overall Reaction Energy (ΔE) for the Conversion of Methane to Methanol by CrO^+ at Several Levels of Theory.

Method	ΔE
B3LYP/DZVP	−17.5
B3LYP*/DZVP	−13.1
B3LYP//B3LYP	−15.7
BP86/DZVP	1.5
CCSD(T)/B3LYP	−11.5
Exp[a]	−3.0 ± 3.0

All the values are in kcal/mol.
[a]Ref. 10i.

experimentally estimated, of −3.0 ± 3.0 kcal/mol,[10i] this thermochemistry was calculated by using value of D_0° (M—O^+)[77]; D_0° (H3C—OH) = 3.911 eV$\Delta_f H_0^\circ$ (CH_3OH)[78]; $\Delta_f H_0^\circ$ (CH3) and $\Delta_f H_0^\circ$ (OH) and D_0° (CH3—H) = 4.48 ± 0.01 eV given and calculated from thermochemistry,[79] and previously theoretically predicted, of −1.3 kcal/mol.[46] In Table 2 are listed, with the aim of comparison, the reaction energies obtained at all the levels of the theory employed in this study. The reaction is predicted to be slightly endothermic at BP86 level, whereas the B3LYP* functional performs better than the B3LYP in this case and gives a reaction energy closer both to the experimental and CCSD(T) values. The overall conversion process of methane to methanol along the spin conserving quartet surface is endothermic of 26.1 kcal/mol, strongly suggesting that the nonadiabatic process is very likely to occur.

Dehydration of methane process takes place through the same steps as conversion to methanol until formation of the insertion intermediate H–CrO^+–CH_3. Thereafter, a second hydrogen migration from carbon to oxygen, corresponding to a four-center transition state, TS2, yields the intermediate H_2O–Cr^+–CH_2, from which the reaction can proceed toward elimination of a water molecule through a simple cleavage of the Cr—O bond. Along the quartet pathway the barrier for the second transition state is below the reactants dissociation limit of only 1.1 kcal/mol and product formation is endothermic of 8.9 kcal/mol. No spin crossing in this case occurs, and the energy diagram for the sextet state parallels that for the quartet being only slightly higher in energy.

Finally, let us look at the reaction pathway for hydrogen elimination. After the electrostatic interaction produces the entrance channel ion–molecule complex CrO^+–CH_4 the energetics of the process is completely unfavorable because two hydrogen shifts from carbon to chromium have to occur. It seems,[33] indeed, that during the C—H bond activation of an alkane R—H by a metal oxide the formation of a strong O—H bond provides the driving force for further reactions. This kind of behavior was detected for first-row transition metal oxides, while the corresponding third-row oxides can exhibit a different reactivity.[43] Therefore, the addition process is much more likely to yield the insertion intermediate HO–M^+–R than the isomeric H–M^+–OR or H–$M(O)^+$–R species. The theoretical work of Yoshizawa et al.[48] on the interaction of methane with iron oxide cation shows that the hydrogen shift from carbon to oxygen is highly favored with respect to the transfer to iron. The height of the barriers that is necessary to surmount and the instability of intermediates that are formed along the way confirm that dehydrogenation hardly occur. The energetic diagram for the excited sextet state was not examined for reasons that appear obvious at an inspection of Figure 2.

Activation of the Methane C—H Bond by CrO_2^+

Experimental studies[36] of the reactivity of chromium dioxide cation toward methane give the following products distribution:

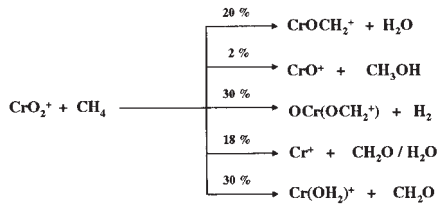

The obtained products pattern shows that the losses of neutral H_2O, H_2, CH_2O, and "CH_4O_2" moiety all occur, being the key products formed by loss of dihydrogen, formaldehyde, and water molecules. A minor pathway leads to the formation of the monoxide CrO^+ by elimination of methanol.

A reaction pattern that accounts for all the observed products is shown in Scheme 1.

In that scheme the key role is played by intermediate (**IV**) that can be formed either from the insertion product (**II**) through an H transfer or from complex (**III**) by a CH_3 transfer. With respect to the scheme proposed in ref. 36 we rule out the possibility that the same intermediate (**IV**) can be directly formed from the initial ion–molecule complex (**I**) with a concerted mechanism. Indeed, all the attempts to locate a transition state for the rearrangement leading to the addition of the CH_3—H bond to the oxygen termini were unsuccessful. All the other conceivable pathways have been theoretically explored in detail in terms of energetically most favorable formation of possible intermediates and barrier heights for transition states leading to them. PESs calculated at B3LYP/DZVP level for both the ground doublet and the quartet excited state of dioxide chromium cation are reported. Figures 3, 4, and 5 show the computed energy diagrams for hydrogen, methanol, and H_2O/CH_2O elimination, respectively. In the same figures are reported relative Gibbs free energies at 298.15 K (ΔG) obtained adding thermal corrections and entropic contributions. We will before illustrate the mechanistic details of the process obtained using the B3LYP/DZVP approach and then the changes introduced into the methane activation PESs by the use of the other approaches. Reoptimization of all species undertaken using B3LYP* and BP86 functionals gives structures only slightly different with respect to those optimized at B3LYP level and for this reason the geometrical changes will not be commented. On the other hand, marked differences are observed in the corresponding potential energy surfaces. In Tables 3 and 4 are compared the relative energies of minima and transitions states with respect to the reactants dissociation limit obtained at different levels of theory. CCSD(T) results are also reported even if the values of T1 diagnostics are much higher than 0.02, and for some structures calculations did not converge.

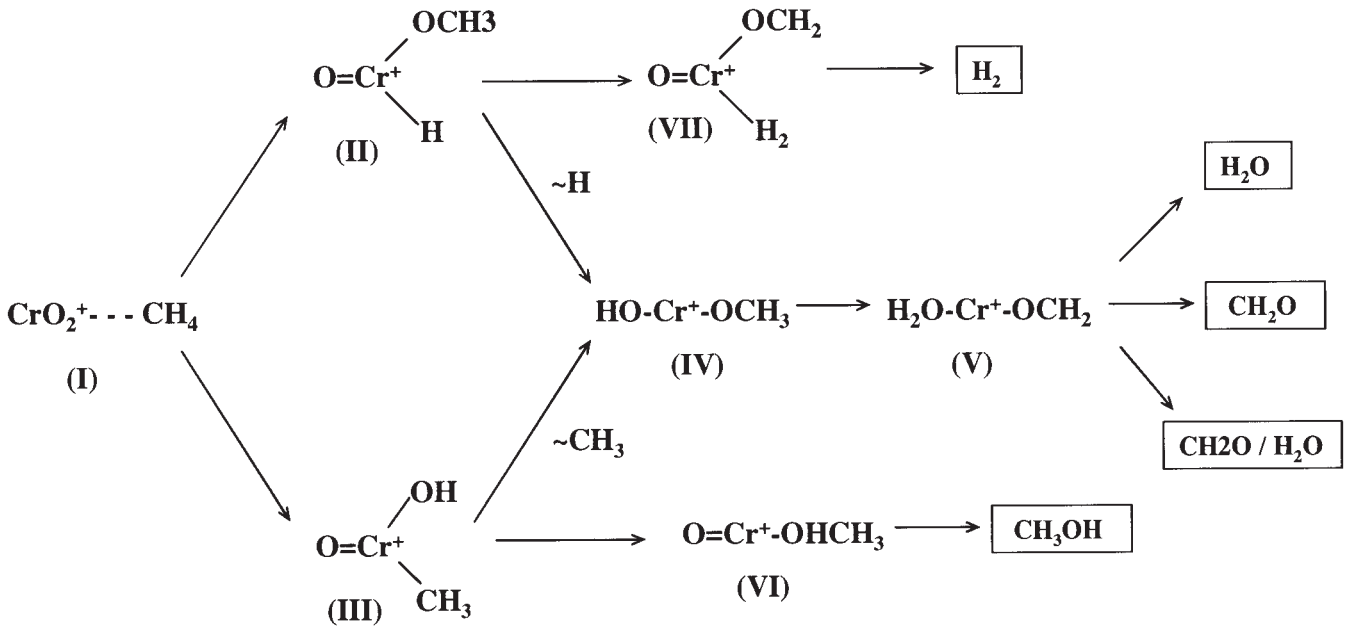

Scheme 1.

B3LYP/DZVP geometric details of minima and transition states, for both doublet and quartet multiplicities, are given in Figures 6 and 7, respectively.

As the very first step of the oxidation of methane by CrO_2^+, reactants come into contact to form the initial ion–molecule complex (**I**), whose most stable structure exhibits a η^3–CH_4 binding mode. With respect to the entrance channel, electrostatic interaction stabilizes a little more the doublet state than the quartet one, and the energy separation becomes 24.4 kcal/mol. From this encounter complex reaction proceeds to give two different insertion complexes, which later on can generate the common intermediate (**IV**). The first one, (**II**), is obtained by a hydrogen shift from carbon to the metal and a contemporary transfer of the CH_3 group to one oxygen terminus. The activation barrier for the three-center transition state (**TSI/II**) associated to this process is 17.4 kcal/mol above the entrance level of the isolated reactants along the doublet surface. Because four of the five 3d electrons of chromium are involved in covalent bonds, intermediate (**II**) exhibits a doublet ground state and is stable as much as the initial ion–molecule complex. The next step, along the path that leads to hydrogen

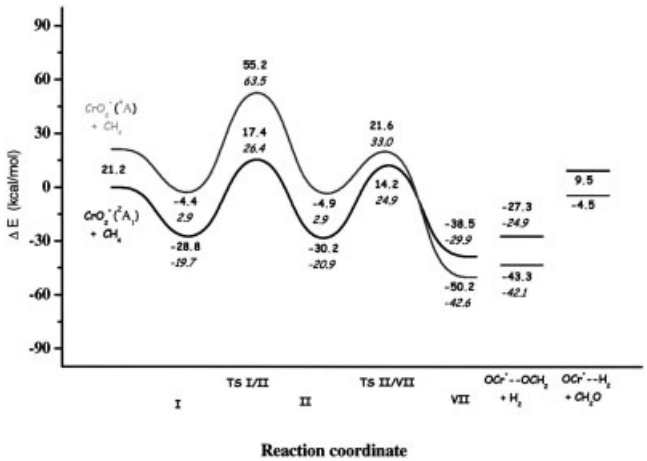

Figure 3. B3LYP/DZVP potential energy surfaces for the reaction of doublet and quartet states of CrO_2^+ cation with CH_4 for hydrogen elimination. Values of Gibbs free energy changes are also reported (numbers in italics). Energies are in kcal/mol and relative to the ground-state reactants.

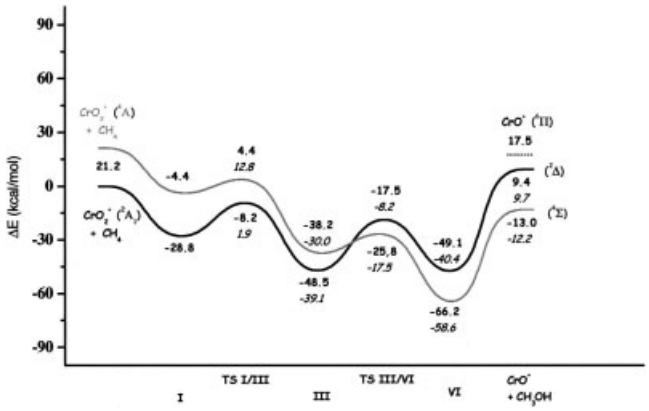

Figure 4. B3LYP/DZVP potential energy surfaces for the reaction of doublet and quartet states of CrO_2^+ cation with CH_4 for conversion to methanol. Values of Gibbs free energy changes are also reported (numbers in italics). Energies are in kcal/mol and relative to the ground-state reactants.

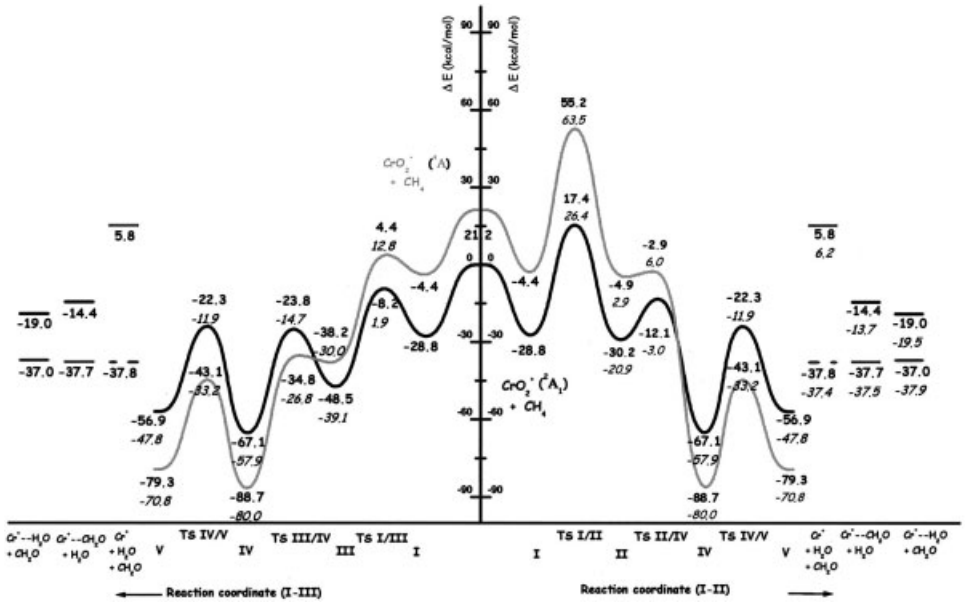

Figure 5. B3LYP/DZVP potential energy surfaces for the reaction of doublet and quartet states of CrO_2^+ cation with CH_4 for elimination of H_2O and CH_2O. The left energy diagram (reaction coordinate I–III) is relative to the path that involves formation of intermediate **III** and the right energy diagram (reaction coordinate I–II) is relative to the path that involves formation of intermediate **II**. Values of Gibbs free energy changes are also reported (numbers in italics). Energies are in kcal/mol and relative to the ground-state reactants.

elimination, consists of a hydrogen transfer from the methoxy group again to the chromium ion with formation, exothermic by 50.2 kcal/mol, of a stable intermediate (**VII**) that represents the direct precursor to molecular hydrogen elimination. Indeed, as can be realized from geometrical parameters in Figure 6, the hydrogen molecule is practically formed yet, and an electrostatic interaction holds together the molecule and the $OCr(OCH_2)^+$ ion. The barrier, corresponding to the four-center transition state (**TSII/VII**) characterized by an almost fully formed H—H bond, is of 14.2 kcal/mol in excess with respect to the energy of the entrance channel dissociation limit. The computed structure of this transition state appears to be more stable in a doublet state, whereas intermediate (**VII**) exhibits a quartet ground state; therefore, the system must undergo a spin inversion that takes place after passage of the transition state. Such a kind of spin crossover, however, does not play a major mechanistic role, and is not considered a rate-limiting factor[33] because it involves species that are formed with excess energy, and even electronically excited states become accessible. Products are directly formed from the $(H_2)OCr(OCH_2)^+$ complex in a barrierless process, with the overall exothermicity of the reaction of 43.3 kcal/mol. These theoretical results confirm that the formaldehyde complex of chromium oxide is formed along the pathway and is more stable in a quartet state. The presence of the formaldehyde ligand lowers the splitting between the doublet and quartet states of CrO^+ cation, from 23.6 to 16.0 kcal/mol, of an amount that is not enough to invert the stability order of the two states. It is worthwhile to note that from the intermediate (**VII**) formaldehyde can also be released with production of the hydrogen chromium oxide complex $(H_2)OCr^+$, even if the reaction is exothermic by only 4.5 kcal/mol.

The data reported in Table 4 results in the fact that no significant change is introduced by the use of both different functionals with the same basis set and the same functional with a more extended basis set. The same general considerations hold for the CCSD(T) results. In comparison with B3LYP/DZVP results, no inversion of the stability order between doublet and quartet states of each species is observed and the transition states remain well above the energy of the separated reactants. It is worth noting that products are destabilized somewhat with respect to reactants with a corresponding decrease of the overall energies of reaction. At the BP86 level all the intermediates are higher in energy and the overall reaction energy is decreased by 26.9 kcal/mol when the products in the quartet ground state are considered. More pronounced are both the trend of destabilization of the transition states and the decrease of the reaction exothermicity observed at the CCSD(T) level.

In Figure 4 are depicted the PESs for the methanol elimination that, from an experimental viewpoint, results to be only a very minor product channel. In this case, the reaction proceeds through the intermediate (**III**), which is obtained starting from the initial ion–dipole complex by a hydrogen shift from carbon to one of the oxygen atoms. Because, also in this case, only one of the five 5d electrons of chromium is not involved into the formation of covalent bonds, the spin is conserved along the path. The four-center transition state (**TSI/III**) for the hydrogen transfer along the low-spin surface lies 8.2 kcal/mol below the entrance channel of separated methane, and CrO_2^+ and the resulting complex (**III**) is stabilized by 48.5 kcal/mol relative to the entrance channel. It is worth noting that formation of intermediate (**III**) with respect to (**II**) is favored from both kinetic and thermodynamic points of

Table 3. Relative Energies of Minima and Transition States (ΔE) Localized along the Paths Leading to H_2O/CH_2O and CH_3OH Elimination through Formation of Intermediate **III** at Several Levels of Theory.

Species	B3LYP/DZVP	BP86/DZVP	B3LYP*/DZVP	B3LYP//B3LYP	CCSD(T)//B3LYP
CrO_2^+ ($^2A_1$)+CH_4	0.0	0.0	0.0	0.0	0.0
CrO_2^+($^4A''$)+CH_4	21.2	36.4	25.1	19.6	27.3
I (^2A)	−28.8	−31.6	−30.4	−30.1	−33.5
I (^4A)	−4.4	−8.5	−1.5	−6.2	−2.4
TSI/III (^2A)	−8.2	−13.4	−10.5	−8.6	−2.4
TSI/III (^4A)	4.4	14.5	6.27	2.9	56.7
III (^2A)	−48.5	−43.3	−49.1	−48.0	−43.9
III (^4A)	−38.2	−23.9	−35.1	−38.7	−30.3
TSIII/VI (^2A)	−17.5	−3.7	−13.3	−6.7	−11.1
TSIII/VI (^4A)	−25.8	−10.9	−22.9	−23.7	−13.7
VI (^2A)	−49.1	−23.8	−49.1	−34.7	−36.3
VI (^4A)	−66.2	−39.51	−60.6	−59.3	−53.2
CrO^+($^2\Delta$) + CH_3OH	9.4	28.7	15.4	12.0	18.8
CrO^+($^4\Pi$) + CH_3OH	−13.0	17.7	−4.6	−3.1	−1.0
TSIII/IV (^2A)	−23.8	−9.5	−20.9	−22.8	−6.3
TSIII/IV (^4A)	−34.8	−19.6	−31.6	−34.6	−26.9
IV (^2A)	−67.1	−43.2	−46.1	−68.34	—
IV (^4A)	−88.7	−63.3	−83.2	−88.8	−73.8
TSIV/V (^2A)	−22.3	−2.4	−17.7	−17.1	−4.4
TSIV/V (^4A)	−43.1	−20.2	−37.8	−37.8	−25.0
TSIII/IV* (^2A)	−10.1	−6.3	−8.9	−9.5	−13.1
TSIII/IV* (^4A)	−8.6	3.4	−6.2	−7.5	2.3
IV* (^2A)	−46.5	−36.1	−44.6	−41.9	−32.8
IV* (^4A)	−37.9	−21.1	−34.4	−33.9	−21.6
TSIV*/V (^2A)	−15.4	−9.6	−21.3	−24.4	−5.2
TSIV*/V (^4A)	−29.9	−8.8	−25.4	−23.4	—
V (^2A)	−56.9	−36.1	−49.1	−46.3	−32.7
V (^4A)	−79.3	−49.4	−72.3	−70.4	−61.6
$CrOH_2^+$ (^2A) + CH_2O	−19.0	50.5	−10.7	−4.12	—
$CrOH_2^+$ (^4A) + CH_2O	−37.0	12.5	−21.2	−25.4	−3.8
$CrOCH_2^+$ (^2A) + H_2O	−14.4	13.4	−7.3	−4.2	—
$CrOCH_2^+$ (^4A) + H_2O	−37.7	−7.9	−30.1	−27.1	−17.2
Cr^+(^6S) + CH_2O + H_2O	−37.8	12.5	−24.8	−24.3	−16.6
Cr^+(^4D) + CH_2O + H_2O	5.8	50.5	14.6	14.5	30.6

All the values are in kcal/mol.

view. The next step of the reaction consists in the rearrangement of complex (**III**) to give intermediate (**VI**) via the three-centered transition state (**TSIII/VI**) corresponding to the migration of the methyl group to give the exit channel complex (**VI**), $OCr(CH_3OH)^+$, which subsequently dissociates to final products. Complex (**VI**) in its quartet state is more stable with 17.1 kcal/mol than the corresponding doublet, and because the transition state is more stable in a quartet spin state, the potential energy surfaces, as shown in Figure 4, cross in a region between structure (**III**) and the transition state (**TSIII/VI**). Accordingly, both doublet and quartet surfaces are relevant for the reaction evolving through the (**TSIII/VI**) transition state. Intermediate (**VI**) directly generates, by breaking of the Cr—O bond without an energy barrier, the reaction products, that is CrO^+ ($^4\Pi$) and methanol. Products formation is predicted to be exothermic by 13 kcal/mol with respect to the entrance channel, if spin change is admitted to take place.

Also for the reaction path that leads to the elimination of methanol the qualitative description obtained at B3LYP/DZVP level remains substantially unchanged when the other computational protocols are used and the use of the BP86 functional gives the most remarkable differences, except a very high energy barrier for the excited state of the **TSI/III** obtained at the CCSD(T) level. Besides a general destabilization of the intermediates, on changing the functional from B3LYP to BP86 the reaction is calculated to be less exothermic by 30.70 kcal/mol and becomes endothermic (see Table 3). The reaction appears to be only slightly exothermic when CCSD(T) calculations are performed as a consequence of a destabilization of about 13 kcal/mol, in comparison with B3LYP/DZVP results, of the last intermediate **VI**.

From both the (**II**) and (**III**) intermediates in their ground doublet states can be formed the complex $(OH)Cr(OCH_3)^+$, which exhibits a quartet ground state and represents the global minimum of the methane/CrO_2^+ system. Therefore, the potential energy curves have to cross along both the pathways. In Figure 5 are plotted the energy diagrams for the paths leading to formation of intermediate (**V**) from both (**II**) and (**III**) intermediates. The transition state **TSII/IV**, which

Table 4. Relative Energies of Minima and Transition States (ΔE) Localized along the Paths Leading to H_2O/CH_2O and H_2 Elimination Through Formation of Intermediate **II** at Several Levels of Theory.

Species	B3LYP/DZVP	BP86/DZVP	B3LYP*/DZVP	B3LYP//B3LYP	CCSD(T)//B3LYP
CrO_2^+ ($^2A_1$)+CH_4	0.0	0.0	0.0	0.0	0.0
I (^2A)	−28.8	−31.6	−30.4	−30.1	−33.5
I (^4A)	−4.4	−8.5	−1.5	−6.2	−2.4
TSI/II (^2A)	17.4	15.4	15.8	18.7	25.8
TSI/II (^4A)	55.2	64.5	57.8	56.9	—
II (^2A)	−30.2	−29.5	−31.0	−29.2	−20.2
II (^4A)	−4.9	18.4	−1.8	−2.1	6.1
TSII/VII (^2A)	14.2	16.0	14.6	18.4	22.4
TSII/VII (^4A)	21.6	26.2	9.5	15.3	32.6
VII (^2A)	−38.5	−22.6	−35.6	−33.3	−22.3
VII (^4A)	−50.2	−25.5	−44.4	−45.6	−37.4
$CrO_2CH_2^+$ (^2A) + H_2	−27.3	10.2	−18.7	−15.2	—
$CrO_2CH_2^+$ (^4A) + H_2	−43.3	−16.4	−36.8	−37.3	−1.7
TSII/IV (^2A)	−12.1	−5.1	−11.6	−9.6	−7.7
TSII/IV (^4A)	−2.9	6.3	−1.6	−0.1	10.6

All the values are in kcal/mol.

leads from complex (**II**) to (**IV**) by a hydrogen transfer from the metal to the oxygen atom, is more stable in a doublet ground state and the curve crossing occurs after the passage of the TS. On the contrary, along the path leading to (**IV**) from (**III**) through CH_3 migration from the metal to the oxygen atom, spin crossing has to take place before the passage of TS as it is more stable in a quartet ground state. Once complex (**IV**) is formed it can undergo a hydrogen transfer from carbon of the methoxy ligand to the oxygen of the hydroxyl group to give, in a spin allowed way, the bis-ligated complex (**V**), $(H_2O)Cr(OCH_2)^+$, which is stabilized by 79.3 kcal/mol with respect to the energy of the entrance channel. This rearrangement proceeds via a four-centered transition state, **TSIV/V**, whose energy is well below that of the separate reactants CrO_2^+ ($^2A_1$), and CH_4. As can be hypothesized, formation of intermediate (**V**) can occur also by hydrogen migration from the methyl unit to the hydroxyl one of intermediate (**III**) with formation of a new intermediate complex (**IV***), $(H_2O)CrO(CH_2)^+$, conserving the spin. From intermediate (**IV***) the reaction proceeds to give complex (**V**) through the migration of the CH_2 group from the metal to the oxygen terminus. Due to the change of the spin state a crossover between doublet and quartet surface has to occur in this region and, because the transition state (**TSIV*/V**) is more stable in a quartet ground state, the required spin change takes place before the passage over the transition state. In Figure 8 is sketched the potential energy diagram for the steps corresponding to the formation of intermediate (**V**) from (**III**) passing through production of intermediate (**IV***) and, as appears at a first glance, this pathway is highly disfavored, both energetically and kinetically, with respect that involving intermediate (**IV**).

With reference to the B3LYP/DZVP PESs, the most marked differences obtained varying the computational approach concern again the results at BP86 level (see Tables 3 and 4). Both spin states of all the intermediates localized along the paths appear to be less stable, and transition states lie higher in energy with respect to the dissociation limit of reactants. To a lesser extent the same behavior is observed for CCSD(T) results.

Products formation from complex (**V**) occurs by barrierless breaking of the bonds to give neutral H_2O, CH_2O, or both. Obviously, in the last case the production of the neutral moiety "CH_4O_2" involves necessary spin inversion on the way as the quartet excited state of chromium cation is higher in energy of with respect to the sextet one. As shown in Figure 5, all the mentioned neutral products can be eliminated in reactions that are exothermic at the B3LYP/DZVP level by the same amount of energy, which is about 37 kcal/mol, and no preference, indeed, is given to one of them. Differences, instead, are introduced by the use of BP86 and B3LYP* functionals, CCSD(T) approach and, even less pronounced, of the TZVP+G(3df,2p) basis set. The more exothermic reaction results to be that leading to the loss of water at all the considered levels of theory. Although the calculated B3LYP exothermicities do not account for the reported yields, the other approaches give results that contradict the experimental findings. The reactions that lead to the loss of formaldehyde and of "CH_4O_2" are calculated to be even endothermic at BP86 level.

From an analysis of the investigated PESs some important features can be outlined. Along all the pathways the involved systems can undergo spin inversions. However, the role that the spin inversions play is probably not crucial because in all the considered situations they occur after the step that appears to be the rate-determining one for the reactions. The activation barriers associated with the formation of the intermediates (**II**) and (**III**), from the first ion–molecule complex, are calculated to be the more energy-demanding and then rate limiting. With regard to these barriers a relevant difference exists, being the **TSI/II** barrier above and the **TSI/III** barrier below the reactants dissociation limit. The importance of spin crossings has to be furthermore examined, taking into account the region where they presumably occur. Indeed, along the paths that involve intermediate (**II**) they are localized in the region between the transition state and intermediate products. On the contrary, once the barrier relative to the formation of intermediate (**III**) is surmounted, spin changes along

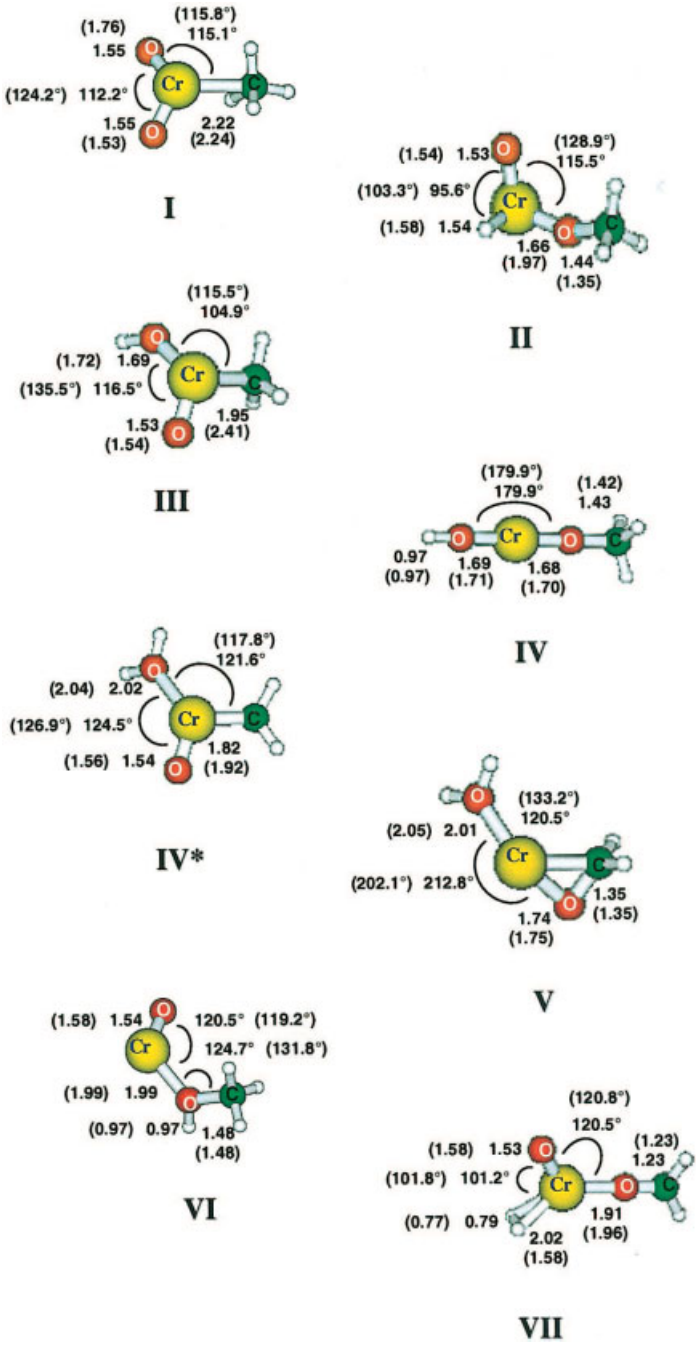

Figure 6. Geometrical parameters of minima localized along the B3LYP/DZVP doublet potential energy surfaces for the reaction of CrO_2^+ with CH_4. The corresponding values for the quartet structures are reported in parentheses. Bond lengths are in angstrom and angles in degrees.

the paths happen before the passage of the transition states. Formation of all the products is predicted to be exothermic. The less exothermic reaction is that leading to methanol formation, while the most energetically favored is that for the hydrogen elimination. Nevertheless, the loss of H_2 goes necessary through formation of intermediate (**II**) and then involves the overcoming of the highest barrier calculated for this reaction pattern and spin crossing between surfaces occurring after TS formation. All the attempts to find an alternative pathway, at a lower energetical cost, for the elimination of molecular hydrogen were unsuccessful. This picture clearly demonstrates that a right balance among all these effects is responsible of the observed distribution of products.

This description of the reaction channels, except the calculated exothermicities of the elimination reactions of H_2O, CH_2O, or

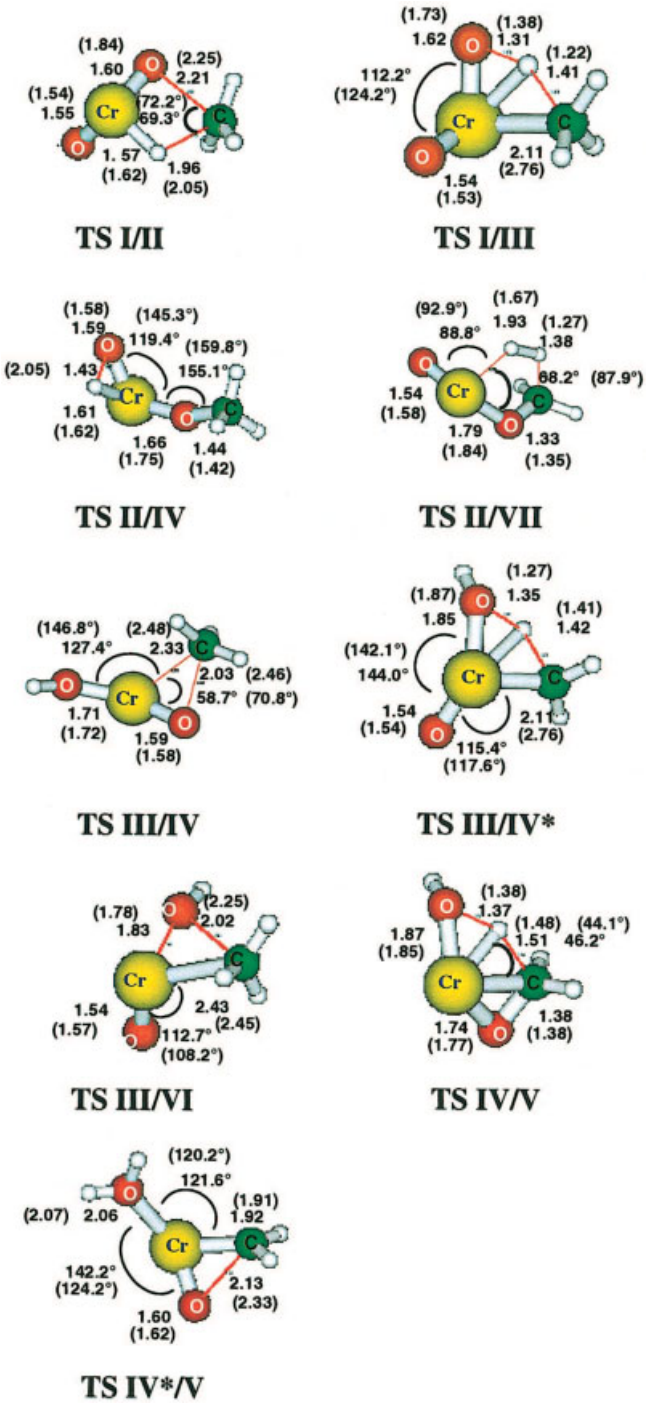

Figure 7. Geometrical parameters of transition states localized along the B3LYP/DZVP doublet potential energy surfaces for the reaction of CrO_2^+ with CH_4. The corresponding values for the quartet structures are reported in parentheses. Bond lengths are in angstrom and angles in degrees. [Color figure can be viewed in the online issue, which is available at www.interscience.wiley.com.]

both, is confirmed by the B3LYP* results, and by the use of a more extended basis set of triple-zeta quality. At BP86 level, in general, intermediates and transition states are calculated to be less stable. This destabilization also lowers the reaction energies to such an extent that the sign of some of them is changed in disagreement with the experimental findings. Destabilization of intermediates and transition states, even less pronounced, is observed also when single-point CCSD(T) calculations are carried out. Therefore, to assess the applicability of the B3LYP* functional to the study of this kind of systems further tests are required, whereas the use of the BP86 functional is not recommended in this case. Results obtained at CCSD(T) level, bearing in mind the high values generally obtained for T1 diagnostics, do not support any particular approach, and in some cases appear to contradict the experimental data.

Some indications on the influence of the temperature on the reactivity pattern described above can be outlined considering energy profiles in terms of Gibbs free energies instead of potential energies. As is shown by the reported B3LYP/DZVP ΔG values in Figures 3, 4, 5, and 8, all the considered reaction channels are spontaneous ($\Delta G < 0$) at 298.15 K. On the contrary, formation of intermediates and transition states from separated reactants is disfavored by entropy by ca. 8–10 kcal/mol at room temperature due to the loss of translational degrees of freedom. Therefore, an overall destabilization of minima and an increase of the energy barriers for the transition states leading to them is observed at 298.15 K. This effect is particularly dramatic for the transition states **TSI/II, TSII/VII**, and **TSI/III**, which lie already above or slightly below the zero energy at 0 K and seem to become less accessible at room temperature. However, the description of a reaction in terms of free energy profiles can differ considerably from that in terms of the potential energy surfaces at 0 K, even when the same reaction coordinate is used, as has been recently shown.[80–83] Although to better understand chemical reactions one should work on free energy surfaces, as geometry optimization of stationary points on the free energy surfaces are not yet a routine task, the number of works concerning this subject is very limited.

Comparison of PESs for H_2 Elimination

In this final section we briefly examine the difference in reactivity with respect to methane activation exhibited by Cr^+, CrO^+, and CrO_2^+ cations comparing their behaviors along the calculated paths leading to the hydrogen elimination, reaction that could be detected for all these three species. In Figure 9 is sketched the PES relative to the methane dehydrogenation process by Cr^+, for comparison with the analogous PESs for CrO^+ and CrO_2^+ reported at the bottom of Figure 2 and in Figure 3, respectively.

The ion–molecule complex is a stable species along the paths of the considered reactions, even if the exothermicity of its formation increases in going from the bare cation to the dioxide. For the bare and oxide cations, at low kinetic energies, only the formation of the initial ion–molecule complex is possible, being the energy of the other intermediates formed during the reaction is well above the dissociation limit of the reactants. Therefore, the low reactivity of CrO^+ indicates that the addition of the oxo ligand does not change the reactivity of the bare cation with respect to the dehydrogenation of methane. The oxo-chromium carbene structure, $O–Cr^+–CH_2$, of the formed intermediate rather than that of a formaldehyde complex, $Cr^+–(OCH_2)$ indicates that the oxygen atom does not participate to the C—H bond activation to yield

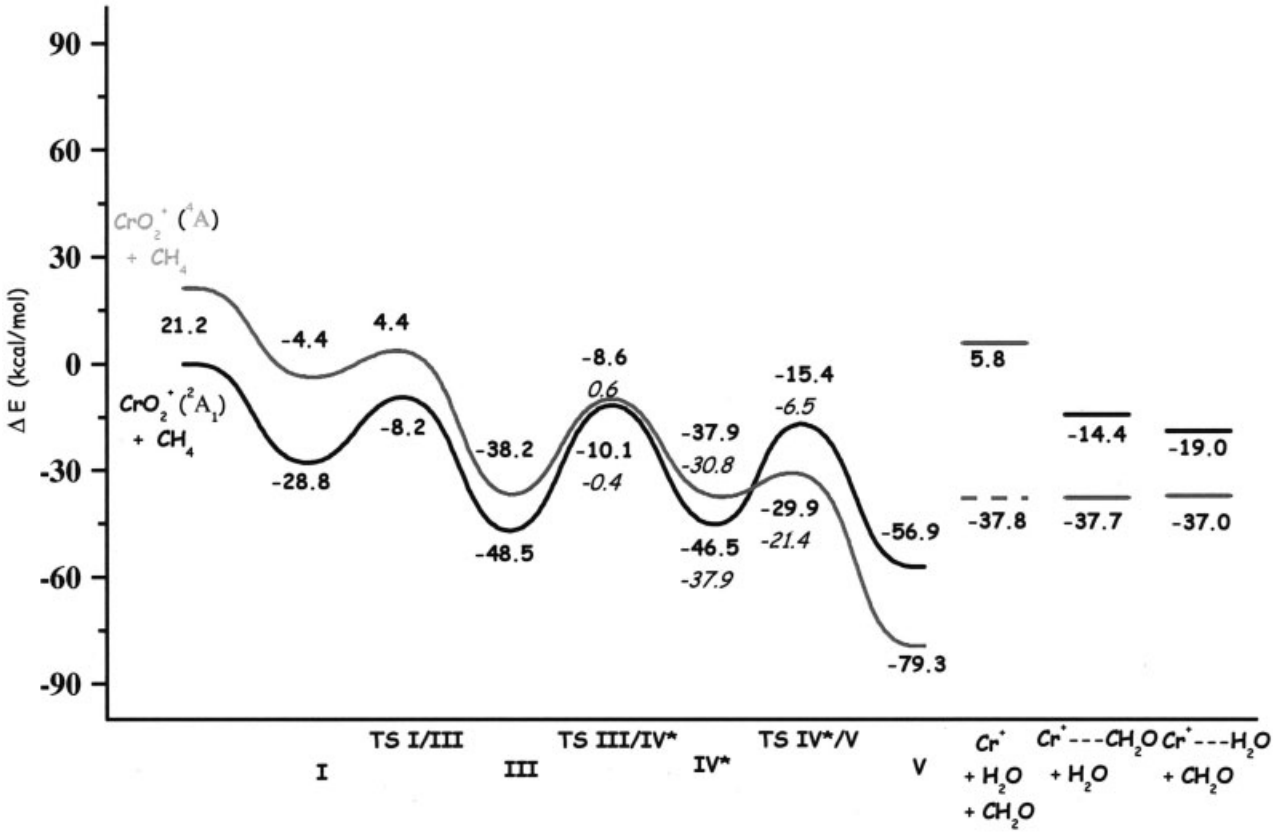

Figure 8. B3LYP/DZVP potential energy surfaces for the reaction of doublet and quartet states of CrO_2^+ cation with CH_4 for elimination of H_2O and CH_2O through formation of intermediate **IV***. Values of Gibbs free energy changes are also reported (numbers in italics). Energies are in kcal/mol and relative to the ground-state reactants.

hydrogen, but instead acts as a spectator ligand. The situation drastically changes when the dioxide cation activates methane. The presence of the second oxo ligand modifies the potential energy surface so that all the reaction intermediates reside in localized minima and become accessible and stable. The direct transfer of hydrogen atoms from carbon to the metal atom can occur and the overall reaction is highly exothermic. It is noteworthy that the first insertion step involves a hydrogen shift from carbon to the metal simultaneously to the insertion of one oxygen atom into the chromium carbon bond so that the second hydrogen is transferred from the formed methoxy group to the metal.

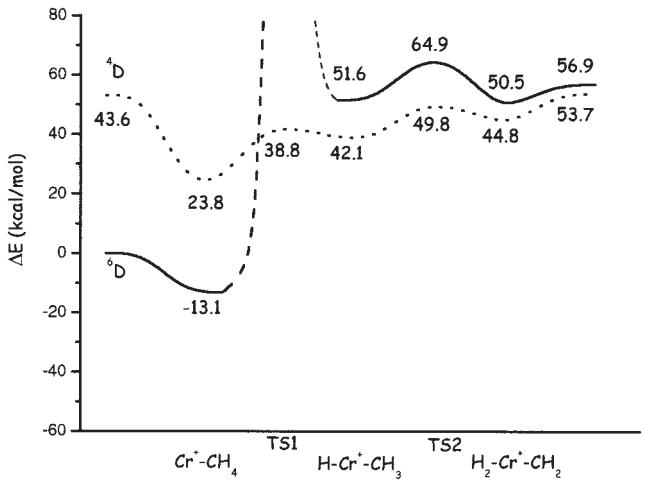

Figure 9. B3LYP/DZVP potential energy surface for the methane activation reaction leading to hydrogen elimination by sextet and quartet states of Cr^+. Energies are in kcal/mol and relative to the ground-state reactants.

Conclusions

The reaction of chromium dioxide cation with methane was analyzed in light of the experimental findings. Both low-spin doublet and high-spin quartet potential energy surfaces for the elimination of neutral H_2, H_2O, CH_2O, and CH_3OH molecules were characterized in detail at the B3LYP level of theory. The reactions occur via multicentered transition states and involve spin crossovers from the entrance channel doublet surface to the quartet one, along which the reaction products are more stable. Spin changes, which are observed to occur before or after the passage of the transition states, of the various product channels probably do not play a significant role, at least not significant as the heights of the activation barriers and the thermodynamic features. The formation of

the hydrogen molecule key product involves direct hydrogen atoms transfer from carbon to the metal atom, reaction that was rarely observed for transition metal monoxide cations. The picture of the mechanistic details of the examined processes remain substantially unchanged when B3LYP* reparametrized functional or a more extended basis set are used. In comparison with B3LYP PESs there are marked differences in the analogous surfaces obtained using the pure BP86 functional that appears to give poor results in the case under study. Single-point CCSD(T) calculations in comparison with B3LYP/DZVP results show a general destabilization of intermediates, transition states, and products, and do not help to reconcile theoretical results with the experiment.

Also, the activation of methane by chromium monoxide cation was studied for both the quartet ground and the sextet excited states with the purpose of comparison. The difference in reactivity with respect to hydrogen elimination in going from bare to mono- to dioxide chromium cations and the enhancement due to sequential ligation was underlined.

In the framework of the complexity of the C—H bond activation mediated by metal oxides, this investigation gives further insight into the mechanistic details of these processes that are far from being satisfactory elucidated.

Supporting Information Available

Figures 1S and 2S containing geometrical parameters of minima and transition states localized along the B3LYP/DZVP sextet and quartet potential energy surfaces for the reaction of CrO^+ with CH_4.

References

1. Shilov, A. E. The Activation of Saturated Hydrocarbons by Transition Metal Complexes; Reidel: Dortrecht, 1984.
2. Russel, D. H., Ed. Gas Phase Inorganic Chemistry; Plenum: New York, 1989, p. 412.
3. (a) Bergman, R. G. Science 1984, 223, 902; (b) Arndtsen, B. A.; Bergman, R. G.; Mobley, T. A.; Peterson, T. H. Acc Chem Res 1995, 28, 154.
4. (a) Armentrout, P. B. Selective Hydrocarbons Activation: Principles and Progress; Davies, J. A.; Watson, P. L.; Greenberg, A.; Liebman, J. F., Eds.; VCH: New York, 1990; (b) Armentrout, P. B. Topics in Organometallic Chemistry; Brown, J. M.; Hofmann, P., Eds.; Springer-Verlag: Berlin, 1999.
5. (a) Crabtree, R. H. The Organometallic Chemistry of the Transition Metals; Wiley: New York, 1994; (b) Crabtree, R. H. Chem Rev 1985, 85, 245; (c) Crabtree, R. H. Chem Rev 1995, 95, 987.
6. (a) Weisshaar, J. C. Adv Chem Phys 1992, 82, 213; (b) Weisshaar, J. C. Acc Chem Res 1993, 26, 213.
7. Lunsford, J. H. Angew Chem Int Ed Engl 1995, 34, 970.
8. Schneider, J. J. Angew Chem Int Ed Engl 1996, 35, 1068.
9. Hall, C.; Perutz, R. N. Chem Rev 1996, 96, 3125.
10. (a) Aristov, N.; Armentrout, P. B. J Phys Chem 1987, 91, 6178; (b) Shultz, R. H.; Elkind, J. L.; Armentrout, P. B. J Am Chem Soc 1988, 110, 411; (c) Sunderlin, L. S.; Armentrout, P. B. J Phys Chem 1988, 92, 1209; (d) Geoorgiadis, R.; Armentrout, P. B. J Phys Chem 1988, 92, 7060; (e) Armentrout, P. B.; Beauchamp, J. L. Acc Chem Res 1989, 22, 315; (f) van Koppen, P. A. M.; Brodbelt–Lustig, J.; Bowers, M. T.; Dearden, D. V.; Beauchamp, J. L.; Fisher, E. R.; Armentrout, P. B. J Am Chem Soc 1990, 112, 5663; (g) Armentrout, P. B. Science 1991, 251, 175; (h) van Koppen, P. A. M.; Brodbelt–Lustig, J.; Bowers, M. T.; Dearden, D. V.; Beauchamp, J. L.; Fisher, E. R.; Armentrout, P. B. J Am Chem Soc 1991, 113, 2359; (i) Clemmer, D. E.; Aristov, N.; Armentrout, P. B. J Phys Chem 1993, 97, 544; (j) Chen, Y.; Armentrout, P. B. J Phys Chem 1995, 99, 10775; (k) Haynes, C. L.; Chen, Y.; Armentrout, P. B. J Phys Chem 1995, 99, 9110.
11. (a) Schröder, D.; Schwarz, H. Angew Chem Int Ed Engl 1990, 29, 1433; (b) Schwarz, H. Angew Chem Int Ed Engl 1991, 30, 820; (c) Schröder, D.; Fiedler, A.; Hrušák, J.; Schwarz, H. J Am Chem Soc 1992, 114, 1215; (d) Fiedler, A.; Hrušák, J.; Koch, W.; Schwarz, H. Chem Phys Lett 1993, 211, 242; (e) Fiedler, A.; Schröder, D.; Shaik, S.; Schwarz, H. J Am Chem Soc 1994, 116, 10734; (f) Wesendrup, R.; Schalley, C. A.; Schröder, D.; Schwarz, H. Chem Eur J 1995, 1, 608; (g) Shaik, S.; Danovich, D.; Fiedler, A.; Schröder, D.; Schwarz, H. Helv Chim Acta 1995, 78, 1393; (h) Ryan, M. F.; Fiedler, A.; Schröder, D.; Schwarz, H. J Am Chem Soc 1995, 117, 2033; (i) Holthausen, M. C.; Fiedler, A.; Schwarz, H.; Koch, W. J Phys Chem 1996, 100, 6236.
12. (a) Saillard, J.-Y.; Hoffmann, R. J Am Chem Soc 1984, 106, 2006; (b) Hoffmann, R. Rev Mod Phys 1988, 60, 601.
13. (a) Koga, N.; Morokuma, K. J Phys Chem 1990, 94, 5454; (b) Koga, N.; Morokuma, K. J Am Chem Soc 1993, 115, 6883; (c) Musaev, D. G.; Koga, N.; Morokuma, K. J Phys Chem 1993, 97, 4064; (d) Musaev, D. G.; Morokuma, K.; Koga, N.; Ngyen, K.; Gordon, M. S.; Cundari, T. R. J Phys Chem 1993, 97, 11435; (e) Musaev, D. G.; Morokuma, K. J Chem Phys 1994, 101, 10697; (f) Musaev, D. G.; Morokuma, K. J Phys Chem 1996, 100, 11600.
14. (a) Low, J. J.; Goddard, W. A., III. J Am Chem Soc 1984, 106, 8321; (b) Low, J. J.; Goddard, W. A., III. J Am Chem Soc 1986, 108, 6115; (c) Perry, J. K.; Ohanessian, G.; Goddard, W. A., III. J Phys Chem 1993, 97, 5238.
15. (a) Blomberg, M. R. A.; Brandemark, U.; Siegbahn, P. E. M. J Am Chem Soc 1983, 105, 5557; (b) Blomberg, M. R. A.; Siegbahn, P. E. M.; Nagashima, U.; Wennerberg, J. J Am Chem Soc 1991, 113, 424; (c) Blomberg, M. R. A.; Siegbahn, P. E. M.; Svensson, M. J Am Chem Soc 1992, 114, 6095; (d) Siegbahn, P. E. M.; Blomberg, M. R. A. Organometallics 1994, 13, 354; (e) Siegbahn, P. E. M. Organometallics 1994, 13, 2833; (f) Siegbahn, P. E. M. J Am Chem Soc 1996, 118, 1487; (g) Siegbahn, P. E. M.; Crabtree, R. H. J Am Chem Soc 1996, 118, 4442.
16. (a) Ziegler, T.; Tschinke, V.; Becke, A. D. J Am Chem Soc 1987, 109, 1351; (b) Ziegler, T.; Tschinke, V.; Fan, L.; Becke, A. D. J Am Chem Soc 1989, 111, 9177; (c) Ziegler, T.; Folga, E.; Berces, A. J Am Chem Soc 1993, 115, 636.
17. (a) Sakaki, S.; Ieki, M. J Am Chem Soc 1991, 113, 5063; (b) Sakaki, S.; Ieki, M. J Am Chem Soc 1993, 115, 2373.
18. (a) Song, J.; Hall, M. B. Organometallics 1993, 12, 3118; (b) Jimenez–Catao, R.; Hall, M. B. Organometallics 1996, 15, 1889; (c) Niu, S.-Q.; Hall, M. B. J Am Chem Soc 1998, 120, 6169.
19. (a) Cundari, T. R. J Am Chem Soc 1992, 114, 10557; (b) Cundari, T. R.; Gordon, M. S. J Am Chem Soc 1993, 115, 4210; (c) Cundari, T. R. J Am Chem Soc 1994, 116, 340.
20. Freas, R. B.; Ridge, D. P. J Am Chem Soc 1980, 102, 7129.
21. Huang, S. K.; Allison, J. Organometallics 1983, 2, 833.
22. Jacobson, D. B.; Freiser, B. S. J Am Chem Soc 1984, 106, 3891.
23. Jackson, T. C.; Jacobson, D. B.; Freiser, B. S. J Am Chem Soc 1984, 106, 1252.
24. Kang, N.; Beauchamp, J. L. J Am Chem Soc 1986, 108, 7502.
25. Eller, K.; Schwarz, H. Chem Rev 1991, 91, 1121.
26. Clemmer, D. E.; Aristov, N.; Armentrout, P. B. J Phys Chem 1993, 97, 544.

27. Pope, R. M.; Buckner, S. W. Org Mass Spectrom 1993, 28, 1616.
28. Clemmer, D. E.; Chen, Y.-M.; Khan, F. A.; Armentrout, P. B. J Phys Chem 1994, 98, 6522.
29. Chen, Y.-M.; Clemmer, D. E.; Armentrout, P. B. J Am Chem Soc 1994, 116, 7815.
30. Bushnell, J. E.; Kemper, P. R.; Maitre, P.; Bowers, M. T. J Am Chem Soc 1994, 116, 9710; Fiedler, A.; Schröder, D.; Shaik, S.; Schwarz, H. J Am Chem Soc 1994, 116, 10734.
31. Ryan, M. F.; Fiedler, A.; Schroder, D.; Schwarz, H. Organometallics 1994, 13, 4072.
32. Schröder, D.; Fiedler, A.; Schwarz, J.; Schwarz, H. Inorg Chem 1994, 33, 5094.
33. Schröder, D.; Schwarz, H. Angew Chem Int Ed Engl 1995, 34, 1973, and references therein.
34. van Koppen, P. A. M.; Kemper, P. R.; Bushnell, J. E.; Bowers, M. T. J Am Chem Soc 1995, 117, 2098.
35. Tjelta, B. L.; Armentrout, P. B. J Am Chem Soc 1995, 117, 5531.
36. Fiedler, A.; Kretzschmar, I.; Schröder, D.; Schwarz, H. J Am Chem Soc 1996, 118, 9941.
37. Kretzschmar, I.; Fiedler, A.; Harvey, J. N.; Schröder, D.; Schwarz, H. J Phys Chem A 1997, 101, 6252.
38. Schwarz, H.; Schröder, D. Pure Appl Chem 2000, 72, 2319, and references therein.
39. Engeser, M.; Schlangen, M.; Schröder, D.; Schwarz, H.; Yumura, T.; Yoshizawa, K. Organometallics 2003, 22, 3933.
40. Schröder, D.; Shaik, S.; Schwarz, H. Acc Chem Res 2000, 33, 139.
41. Armentrout, P. B.; Beauchamp, J. L. Acc Chem Res 1989, 22, 315.
42. Armentrout, P. B. Science 1991, 251, 175.
43. Irikura, K. K.; Beauchamp, J. L. J Am Chem Soc 1989, 111, 75.
44. Cassady, C. J.; McElvany, S. W. Organometallics 1992, 11, 2367.
45. Russo, N.; Sicilia, E. J Am Chem Soc 2002, 124, 1471.
46. Shiota, Y.; Yoshizawa, K. J Am Chem Soc 2000, 122, 12317.
47. Yoshizawa, K.; Shiota, Y.; Yamabe, T. J Am Chem Soc 1998, 120, 564.
48. Yoshizawa, K.; Shiota, Y.; Yamabe, T. Chem Eur J 1997, 3, 1160.
49. Becke, A. D. J Chem Phys 1993, 98, 5648.
50. Stephens, P. J.; Devlin, F. J.; Chabalowski, C. F.; Frisch, M. J. J Phys Chem 1994, 98, 11623.
51. Ricca, A.; Bauschlicher, C. W., Jr. Chem Phys Lett 1995, 245, 150.
52. Bauschlicher, C. W., Jr.; Ricca, A.; Partridge, H.; Langghoff, S. R. In Recent Advances in Density Functional Theory; Chong, D. P., Ed.; World Scientific Publishing Co.: Singapore, 1997; Part II, and references therein.
53. Sodupe, M.; Branchadell, V.; Rosi, M.; Bauschlicher, C. W., Jr. J Phys Chem 1997, 101, 7854.
54. Aschi, M.; Brönstrup, M.; Diefenbach, M.; Harvey, J. N.; Schröder, D.; Schwarz, H. Angew Chem Int Ed Engl 1998, 37, 829.
55. Pavlov, M.; Siegbahn, P. E. M.; Sandström, M. J Phys Chem A 1998, 102, 219.
56. Yi, S. S.; Blomberg, M. R. A.; Siegbahn, P. E. M.; Weisshaar, M. J Phys Chem 1998, 102, 395.
57. Torrent, M.; Sola, M.; Frenking, G. Chem Rev 2000, 100, 439.
58. Niu, S. Q.; Hall, M. B. Chem Rev 2000, 100, 353.
59. Andzelm, J.; Radzio, E.; Salahub, D. R. E. J Comp Chem 1985, 6, 520.
60. Goudbout, N.; Salahub, D. R.; Andzelm, J.; Wimmer, E. Can J Chem 1992, 70, 560.
61. (a) Irigoras, A.; Fowler, J. E.; Ugalde, J. M. J Phys Chem 1998, 102, 293; (b) Irigoras, A.; Fowler, J. E.; Ugalde, J. M. J Am Chem Soc 1999, 121, 574; (c) Irigoras, A.; Fowler, J. E.; Ugalde, J. M. J Am Chem Soc 1999, 121, 8549; (d) Irigoras, A.; Elizalde, O.; Silanes, I.; Fowler, J. E.; Ugalde, J. M. J Am Chem Soc 2000, 122, 114.
62. (a) Russo, N.; Sicilia, E. J Am Chem Soc 2001, 123, 2588; (b) Michelini, M. C.; Russo, N.; Sicilia, E. J Phys Chem 2002, 106, 8937; (c) Michelini, M. C.; Russo, N.; Sicilia, E. Inorg Chem 2004, 43, 4944; (d) Chiodo, S.; Kondakova, O.; Irigoras, A.; Michelini, M. C.; Russo, N.; Sicilia, E.; Ugalde, J. M. J Phys Chem A 2004, 108, 1069.
63. Reiher, M.; Salomon, O.; Hess, B. A. Theor Chem Acc 2001, 107, 48.
64. Salomon, O.; Reiher, M.; Hess, B. A. J Chem Phys 2002, 117, 4729.
65. Cavallo, L.; Jacobsen, H. J Phys Chem A 2003, 107, 546.
66. Jacobsen, H.; Cavallo, L. Phys Chem Chem Phys 2004, 6, 3747.
67. Becke, A. D. Phys Rev A At Mol Opt Phys 1988, 38, 3098.
68. Perdew, J. P. Phys Rev B: Condens Matter Mater Phys 1986, 33, 8822.
69. Boys, S. B.; Bernardi, F. Mol Phys 1970, 19, 553.
70. Frisch, M. J.; Trucks, G. W.; Schlegel, H. B.; Scuseria, G. E.; Robb, M. A.; Cheesman, J. R.; Zakrzewski, V. G.; Montgomery, J. A., Jr.; Stratmann, R. E.; Burant, J. C.; Dapprich, S.; Millam, J. M.; Daniels, A. D.; Kudin, K. N.; Strain, M. C.; Farkas, O.; Tomasi, J.; Barone, V.; Cossi, M.; Cammi, R.; Mennucci, B.; Pomelli, C.; Adamo, C.; Clifford, S.; Ochterski, J.; Petersson, G. A.; Ayala, P. Y.; Cui, Q.; Morokuma, K.; Malick, D. K.; Rabuck, A. D.; Raghavachari, K.; Foresman, J. B.; Cioslowski, J.; Ortiz, J. V.; Stefanov, B. B.; Liu, G.; Liashenko, A.; Piskorz, P.; Komaromi, I.; Gomperts, R.; Martin, R. L.; Fox, D. J.; Keith, T.; Al-Laham, M. A.; Peng, C. Y.; Nanayakkara, A.; Gonzalez, C.; Challacombe, M.; Gill, P. M. W.; Johnson, B. G.; Chen, W.; Wong, M. W.; Andres, J. L.; Head–Gordon, M.; Replogle, E. S.; Pople, J. A. Gaussian 98; Gaussian, Inc.: Pittsburgh, PA, 1998.
71. Lee, T. J.; Rice, J. E.; Scuseria, G. E.; Schaefer, H. F., III. Theor Chem Acc 1989, 75, 81.
72. Lee, T. J.; Taylor, P. R. Int J Quantum Chem 1989, 23S, 199.
73. Moore, C. E. Atomic Energy Levels; NSRD-NBS, USA; U. S. Government Printing Office: Washington, DC, 1991, Vol 1.
74. Dyke, J. M.; Gravenor, B. W. J.; Lewis, R. A.; Morris, A. J Chem Soc Faraday Trans 2 1983, 79, 1083.
75. Harrison, J. F. J Phys Chem 1986, 90, 3313.
76. Jasien, P. G.; Stevens, W. J Chem Phys Lett 1988, 147, 72.
77. Fisher, E. R.; Elkind, J. L.; Clemmer, D. E.; Georgiadis, R.; Loh, S. K.; Aristov, N.; Sunderlin, L. S.; Armentrout, P. B. J Chem Phys 1990, 93, 2676.
78. Wagman, D. D.; Evans, W. H.; Parker, V. B.; Schumm, S. H.; Halow, I.; Bailey, S. M.; Churney, K. L.; Nutall, R. L. J Phys Chem Ref Data 1982, 11 (Suppl. No. 1).
79. Chasc, M. W.; Davies, C. A.; Downey, J. R.; Frurip, D. J.; McDonald, R. A.; Syverud, A. N. J Phys Chem Ref Data 1985, 14 (Suppl. No. 1) (JANAF tables).
80. Ensing, B.; Laio, A.; Gervasio, F. L.; Parrinello, M.; Klein, M. L. J Am Chem Soc 2004, 126, 9492.
81. Ammal, S. C.; Yamataka, H.; Aida, M.; Dupuis, M. Science 2003, 299, 1555.
82. Yang, S.-Y.; Fleurat–Lessard, P.; Hristov, I.; Ziegler, T. J Phys Chem A 2004, 108, 9461.
83. Yang, S.-Y.; Hristov, I.; Fleurat-Lessard, P.; Ziegler, T. J Phys Chem A 2005, 109, 197.